Hindawi Publishing Corporation
Journal of Sensors
Volume 2009, Article ID 402174, 19 pages
doi:10.1155/2009/402174

Review Article

Fabrication of TiO_2 Nanotube Thin Films and Their Gas Sensing Properties

Yongxiang Li, Xiaofeng Yu, and Qunbao Yang

State Key Laboratory of High Performance Ceramics and Superfine Microstructures, Shanghai Institute of Ceramics, Chinese Academy of Sciences, 1295 Dingxi Road, Shanghai 200050, China

Correspondence should be addressed to Yongxiang Li, yxli@mail.sic.ac.cn

Received 3 January 2009; Accepted 28 May 2009

Recommended by Giorgio Sberveglieri

The fabrication process and the growth mechanism of titanium/titania nanotubes prepared by anodization process is reviewed, and their applications in the fields of dye sensitized solar cells, photocatalysts, electrochromic devices, gas sensors, and biomaterials are presented. The anodization of Ti thin films on different substrates and the growth process of anodic titanium oxide are described using the current-time curves. Special attention is paid on the influences of the initial film smoothness on the resulted nanoporous morphologies. The "threshold barrier layer thickness model" is used to discuss the growth mechanism. As a case study for gas sensing, anodized highly ordered TiO_2 nanotube arrays and nanoporous thin films that show porous surface with an average diameter of 25 nm and interpore distance of 40 nm were prepared. Gas sensors based on such nanotube arrays and nanoporous thin films were fabricated, and their sensing properties were investigated. Excellent H_2 gas sensing properties were obtained for sensors prepared from these highly ordered TiO_2 nanotube arrays, which present stable response even at a low operating temperature of 90°C. Based on our experimental results, "H-induced O^{2-} desorption" mechanism was used for explaining the hydrogen gas sensing mechanism.

1. Introduction

Nanoporous structures are of significant importance in a variety of nanostructured because they not only have the common properties that are widely seen in nanomaterials such as surface effect, size effect, and enhanced chemical and optical properties but can also be used as "nano-templates" to fabricate other nanostructures such as nanodots, nanowires and, nanotubes, which further expand their potential applications. In recent years, in line with the increase in research on the development nanomaterials, the properties of a variety of novel functional devices have been largely explored based on the unique optical, mechanical, chemical, and electrical properties of nanomaterials.

It is undoubtedly agreed that anodic alumina oxide (AAO) is one of the most investigated nanostructures and has attracted lots of interests. With the development of AAO and its growth model and mechanism, the anodization process has been adopted to the other metals such as Ti, Ta, Nb, W, Hf, and Zr, and so forth (so called valve metals). Many different nanostructures have been fabricated from those metals, and more applications as well as functionalities have been developed, and are still actively under investigations.

The applications of nanomaterials include photoluminescence [1–11], sensors [12–16], photo-catalysts [17], DSSCs [18–23], high-density vertical magnetic storage [24–30], field emission devices [31–37], rapid response electrochromic devices [38], and so forth. In this review paper, we focus on the recent progresses in the field of anodic titanium nanotube/nanoporous thin film fabrication and its applications in gas sensors.

2. Fabrication of Anodic Titanium Nanotubes

The preparations of TiO_2 nanotubes were reported through hydrothermal synthesis [39, 40] and templated sol-gel process [41]. However, the first report on nanoporous structure of anodized Ti metal can be traced to 1920s. In 1999, Zwilling et al. [42, 43] found that when chromium acid was used

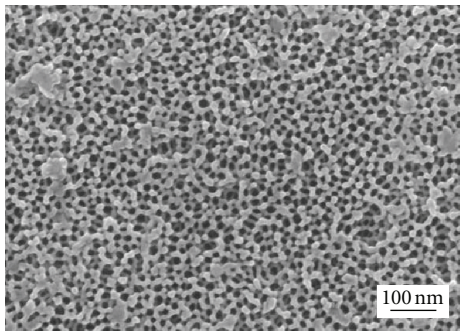

Figure 1: Typical SEM images of anodic titanium oxide (ATO) nanoporous thin film.

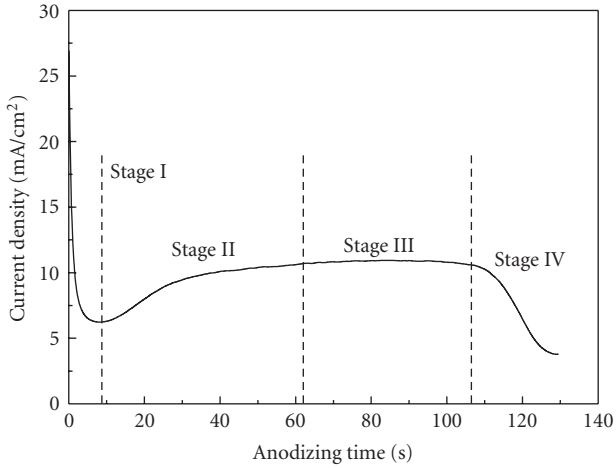

Figure 2: Current transient during the anodization process.

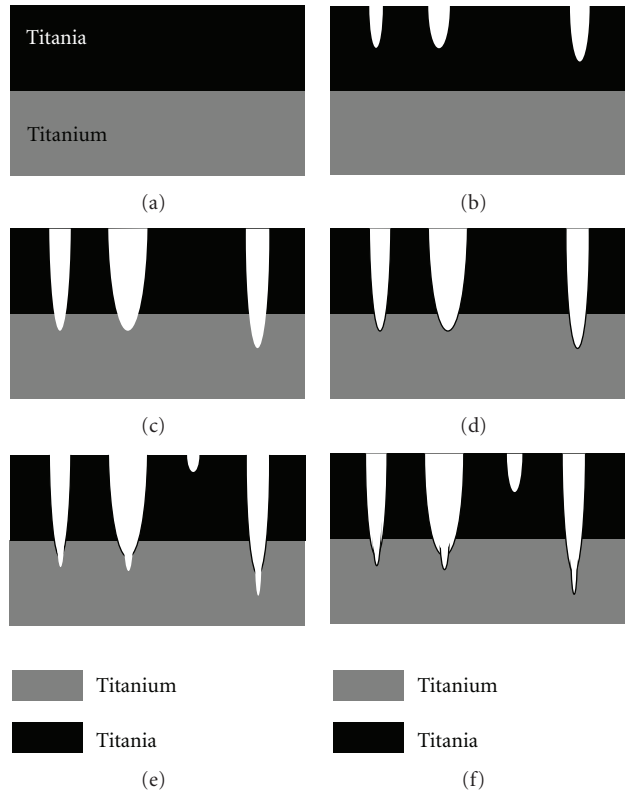

Figure 3: Schematic diagram of the passivation and repassivation effect during the anodization process.

as the electrolyte to perform the anodization on titanium and its alloy (TA6V), a compact oxide film was obtained, while in an HF/chromium acidic electrolyte, a nanoporous structure was obtained instead. In 2001, Grimes and his team reported their systematic research on the nanotubular structures obtained by titanium anodization process. Such an anodization process has since attracted an increasing interest with the establishment of its growth model, crystal structure, and the other relating theories. Meanwhile, a series of functional devices were developed based on such nanostructures.

The development of anodic titanium nanostructures will be reviewed in this paper. Experimental results confirmed that the types of electrolytes as well as the anodizing potential, processing temperature, and reaction time are the key factors that affect the final nanostructures which all will be discussed in this paper. A comprehensive report on the gas sensing properties of such films will also be presented.

2.1. HF Acid-Based Anodization. HF acid is widely used as the electrolyte since it has the highest efficiency for the anodization of titanium, and the anodization parameters were studied and optimized. Gong et al. [44] reported that when 0.5 wt% HF was used, a nanoporous structure was obtained at a relatively low anodizing potential (<3 V) while discrete nanotubular arrays were obtained when the potential >5 V. With increasing the anodizing potential to over 40 V, randomly distributed pores were observed because of the deterioration of the nanotube structure. Their research showed that the electrochemical window for the nanotube formation is in the range from 10 V to 40 V which strongly depended on and related to the concentration of the electrolyte and the applied potential. They also reported that the diameter, wall thickness, and length of the nanotubes increase with the increase of anodizing potentials.

More anodization experiments were performed in HF contained mixture electrolytes. Mor et al. [45–49] reported that when anodization was carried out in the oxalic acid/0.5 wt% HF (1 : 7 in volume ratio), the resulted nanotube did not show a significant difference in diameter and shape except for wall thickening. When anodized at 10 V, the inner diameters of the nanotubes were approximately 20 nm, and the wall thicknesses were ~15 nm. Further study showed that the wall thickness and the tube length are both a function of the anodizing temperature. With decreasing anodizing temperature, because of the low dissolution rate, the wall thickness increases and then causes a high filling between the interspace of neighboring nanotubes which ultimately connects the nanotubes and forms a nanoporous structure. This result proved that, during the anodization process, chemical dissolution and electrochemical etching are the two key processes.

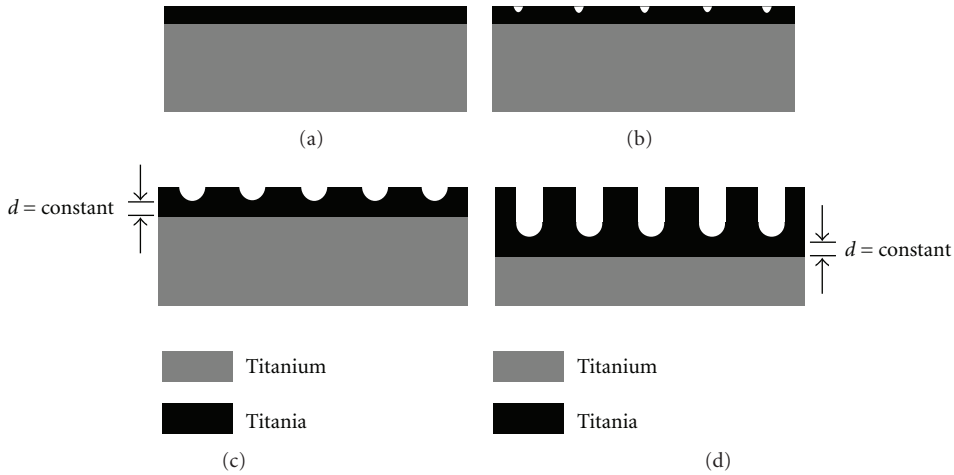

Figure 4: Schematic diagram of the dynamic balance during the anodization process.

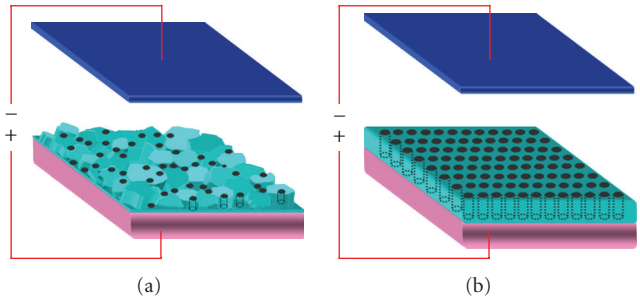

Figure 5: Schematic diagram of the relationship between the surface structure and the final morphology.

Beranek et al. [50] reported the anodization process in H_2SO_4/HF electrolyte. In their report, the anodic current goes smoothly when anodization is performed in H_2SO_4 electrolyte. In HF-electrolyte, however, continuous oscillation occurs, and the scope is related to the concentration. They explained that there exists a competition between oxide formation and dissolution, and HF is the key factor, which causes the dissolution of oxide layer. Such a competition finally results in a length limitation when nanotubes are fabricated in HF contained electrolytes. The study of the relationship between the length of the nanotube and the "competition between oxide formation and dissolution" is very unique. They also observed an oscillation in the anodizing current, but they did not give a reasonable explanation for it.

2.2. Neutral Electrolyte-Based Anodization. As discussed above, Beranek's discussion on the relationship between nanotube length limitation and growth mechanism is very interesting, and such a viewpoint was confirmed by Macak et al. [51, 52] and Bauer [53]. Macak pointed out that there exists a length limitation of several hundred nanometers when anodization is performed in HF-based electrolytes. The reason for such a limitation is the dissolution caused by acidic electrolyte on the top of nanotubes. As a result, in order to obtain nanotubes with a higher aspect ratio (L/D), the dissolution rate at both top and bottom of the nanotube should be adjusted, which means that the formation rate of the nanotube at the bottom should be enhanced while the dissolution of the existed nanotube on the top should be restrained. They realized it by the application of a type of neutral electrolyte, and the nanotubes with extremely large aspect ratio were obtained. The neutral buffered electrolytes used in their experiments were $NH_4F/(NH_4)_2SO_4$ [51] and NaF/Na_2SO_4 [52]. By the application of neutral electrolyte, a low pH value was established at the bottom of the nanotube which enhanced the growth rate, while at the top and wall area of the nanotube, a relatively high pH value prevented the electrochemical dissolution. As a result, the "second generation" nanotube array with large aspect ratio was succeeded. The research which has been performed by Macak to adjust the pH value of the electrolyte at different parts of the nanotubes is of significant importance.

Anodic titanium nanotube arrays with a length of several micron meters were also reported by Grimes et al. [54, 55] when the anodization was performed in a KF (or NaF) electrolyte. According to their results, the pH value has a significant effect on the electrochemical dissolution during the anodization process. Such an effect is caused by the hydrolysis of titanium ions. Usually, longer nanotubes are formed when keeping the pH value of the electrolyte at a high level (< 7). At a given pH value, the length and diameter of the nanotube increase with increasing the anodization potential. However, at a given potential, the diameter is not affected by the pH value.

Cai et al. [54] reported that the extension of anodizing time does not increase the length of the nanotubes when anodization is performed in strong acidic electrolyte ($pH < 1$); in weak acidic electrolyte, however, the tube length increases with the increasing of anodizing time. According to their results, the nanotubes with large aspect ratio can be obtained in a pH range of 3–5. The nanotubes formed in an electrolyte with a low pH value is found to be short but

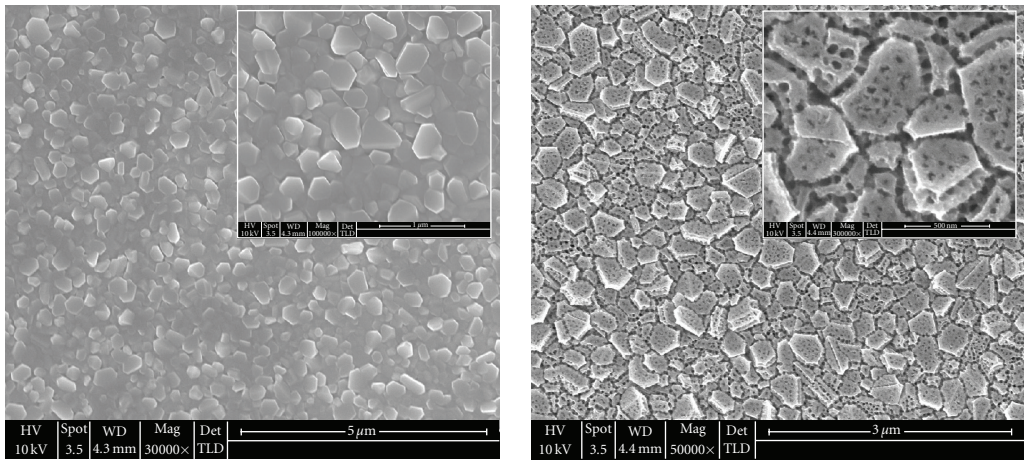

(a) (b)

Figure 6: SEM images of (a) Ti thin film fabricated by RF-sputtering and (b) after anodization in a 0.5 wt% NH_4F/EG electrolyte.

very "clean", while a high pH value may help to form longer nanotubes, severe coverage occurs at the open mouth of the nanotubes, and no nanotubular structure could be formed in alkaline electrolytes. The studies of the effect of pH value on nanostructure morphologies given by Cai and coworkers are systematic, they confirmed again that the competition between formation and dissolution of oxide layer is the key driving force of nanotube growth, and the major factor of the length of final tubes as well.

Macak et al. [56–58] and Richter et al. [59] noticed subtly in their results the regular strips on the outer wall of nanotubes and ascribed such strips to the current oscillations. They explained that when associating anodizing time with the tube length, the frequency of current oscillation exactly matches the distance between the neighboring strips. Based on this assumption, the pH value breaking is the primary cause of the current oscillation and final formation of the strips. Subsequently, they replaced the conventional electrolyte with a high-viscosity electrolyte to control the pH breaking, and the nanotubes with smooth walls were successfully prepared.

2.3. Organic Electrolyte-Based Anodization. With the development of Ti anodization techniques, a variety of electrolytes were investigated to evaluate their effects on the nanostructure morphologies. The electrolytes used are not within the limitation in conventional aqueous solutions but with multiple choices to organic solutions. Tsuchiya et al. [60] reported one type of titanium nanotube arrays with "coral reefs" morphology which is quite different from the previously reported nanostructures. Such nanotube arrays were fabricated at high anodizing potential in F-contained "water-free" acetic acid electrolyte. However, they did not give the explanation of the effect as why the using of acetic acid may result in such a nanostructure.

Ruan et al. [61] formed highly ordered nanotube arrays when performed the anodization in an HF-contained

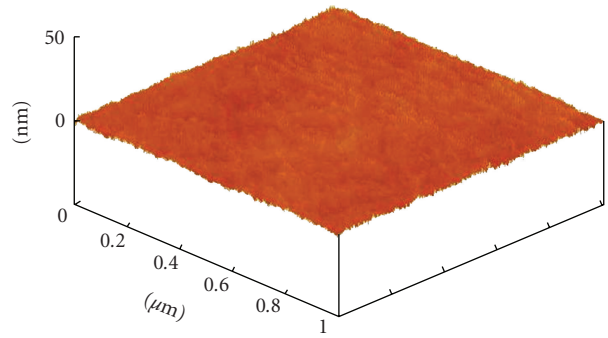

Figure 7: AFM image of Ti thin films fabricated by an FCVA process.

dimethylsulfoxide (DMSO)/ethanol mixture electrolyte. According to their report, the nanotubes obtained in such an electrolyte present an enhanced photoelectric response compared with that formed in conventional aqueous electrolytes. The excellent properties were ascribed to the unique morphologies. However, they did not point out the relationship between the electrolyte and the morphology.

3. Mechanism Model and Crystallization Process

The most widely acceptable growth mechanism of anodic titanium is originated from the growth mechanism of AAO [55]. The formation process of titanium nanotubes is similar to those of AAO including the following procedures: (1) formation of an oxide layer at Ti metal surface when reacting with O^{2-} and OH^- at the anode; after that, the anions diffuse into the oxide layer and continuously react with the metal beneath; (2) migration of Ti^{4+} from the oxide/metal interface to metal/electrolyte interface under the electric field; (3) dissolution at the oxide/electrolyte interface;

Ti-O bond becomes weak under the applied electric field which causes the dissolution; Ti^{4+} goes into the electrolyte while the free O^{2-} ions diffuse across the oxide layer and react with Ti metal at the oxide/metal interface; (4) since acidic electrolytes are most used for the Ti anodization, the chemical dissolution cannot be neglected. In the Ti anodization, nanotubular structures (discrete nanotubes) instead of nanoporous structure are commonly obtained compared with that in Al anodization process.

It is of significant importance to investigate the crystal structure of anodic titanium since it is closely related to its properties and applications. For instance, anatase titanium dioxide is widely used in DSSCs, while TiO_2 with rutile phase finds its applications in gas sensors as a dielectric layer.

The as-prepared anodic titanium is amorphous and crystallizes after annealing process. Varghese et al. [62] investigated the crystallization process of anodic titanium by anodizing titanium in HF electrolyte at 20 V with the following annealing in O_2 at different temperatures. According to their report, anodic titanium remains an amorphous structure when the annealing temperature is below 250°C, and anatase structure appears at the annealing temperature between 250 and 280°C. When the temperature is close to 430°C, rutile phase can be found according to the XRD results. Beyond 430°C, rutile phase becomes dominant,and at annealing temperature between 620 and 680°C, the anodic titanium transfers fully to rutile phase TiO_2. Varghese et al. also investigated the grain size of the anatase TiO_2 as well as the rutile TiO_2 and found that initially the grain size of anatase phase increases with the temperature increasing. It followed by a decrease at 480∼580°C and increases again after 580°C. As for the grain size of rutile phase, it continuously increases with the increasing of annealing temperature. There is 31% rutile phase structure at 430°C and 75% at 480°C; it reaches 91% when annealing temperature is as high as 580°C.

When the anodization was performed in H_3BO_3-HNO_3-HF electrolyte or in HNO_3-HF electrolyte followed by annealing in O_2, very similar results were obtained compared with that in HF electrolyte. In KF (or NaF), the XRD results showed that the anodic titanium remains amorphous below the annealing temperature of 230°C, and not until 280°C it starts to crystallize. The results are exactly the same with the experiments performed in HF aqueous solutions without any added acid. Therefore, one can draws a conclusion that neither the concentration of electrolyte nor the pH value has any effects on the crystallization temperature of titanium nanotubes.

It is worthy to mention that, according to Mor's studies on the anodization of titanium thin film sputtered on glass substrates, when there is discontinuous metal thin film remaining at the bottom of nanotubes, even at an annealing temperature of 500°C, no rutile phase is obtained. Such a result is in contrast with that when anodization was performed on Ti metal sheet/foil. However, when the nanotubes with thick, continuous metal film was annealed, both anatase and rutile were obtained at an annealing temperature of 480°C, which is similar to the XRD results when performing anodization on Ti sheet [54, 63, 64]. Based on these results, Mor et al. gave their assumption that rutile phase only forms at the oxide/metal interface when Ti metal is thermal oxidized, while because of the confinement by the wall of the nanotubes, the increscent nuclear grain size prevents its transformation to rutile phase. This assumption was confirmed by selected area electron diffraction (SAED) when analyzing single nanotube which is annealed at 600°C; anatase instead of rutile phase was observed at the wall of the nanotube.

4. Applications of Anodic Titanium

4.1. Water Photolysis. Grimes and his coworkers [65–68] reported their research on the water photolysis by using anodic titanium nanotube arrays as the anode. By illuminating the nanotube arrays under UV light (320∼400 nm, 100 mW/cm^2) and then investigating the relationship between I-V curve and anodizing temperature, they found that the current density obtained from nanotubes anodized at 1.5 V, 5°C is 3 times higher than that of anodized at 50°C and, low temperature anodization always results in the increasing of the slope in I-V curve. The highest quantum efficiency of 90% is obtained when the sample anodized at 10 V; 5°C is illuminated under 337 nm UV light (2.7 mW/cm^2).

4.2. Dye Sensitized Solar Cells (DSSCs). Mor et al. [69, 70] reported transmitted type of DSSCs based on highly ordered TiO_2 nanotube arrays. In their research, Ti thin film with a thickness of 400 nm was sputtered on an FTO glass substrate followed by an anodization process in 0.5% HF/acetic acid (7 : 1 in volume ratio) electrolyte at 10 V. The obtained nanotube arrays were annealed at 450°C for 3 hours to be transformed to anatase phase. Before being used in DSSCs, the nanotubes were treated in 0.2 M $TiCl_4$ for 1 hour followed by annealing again at 450°C for another 30 minutes. Dye adsorption was realized by dipping the sample into 0.3 mM N719 (Dysol) contained ethanol solution for 12 hours. A 25 nm Pt coated conductive glass was used as the counter electrode and a methoxypropionitrile (MPN) solution containing 0.5 M LiI, 0.05 M I_2, 0.6 M N-methylbenzimidazole, 0.1 M guanidinium thiocyanate, 0.5 M tert-butylpyridine was used as the electrolyte. The effective area for the cell was 0.25 cm^2. At a given length of nanotubes (3.6 μm), the short circuit current (J_{sc}) could reach ∼10.3 mA/cm^2, while an open circuit voltage (V_{oc}) of ∼0.84 V was obtained under an illumination of AM-1.5 (100 mW/cm^2). The filling factor (FF) was 0.54 with a photoconversion efficiency of 4.7%.

Mor et al. [69, 70] mentioned that the photoconversion efficiency increases with the increasing of the tube length and the results obtained in this case (when nanotubes with 3.6 μm length is used) can only be reached when a 10 μm thick conventional nanocrystalline TiO_2 is used. Such a high efficiency is obviously ascribed to the large surface area obtained by the nanotubular structure. But still there are some problems need to be solved in this type of devices. The first one is the dye adsorption efficiency. Since there only exists an open mouth for each nanotube, the remaining

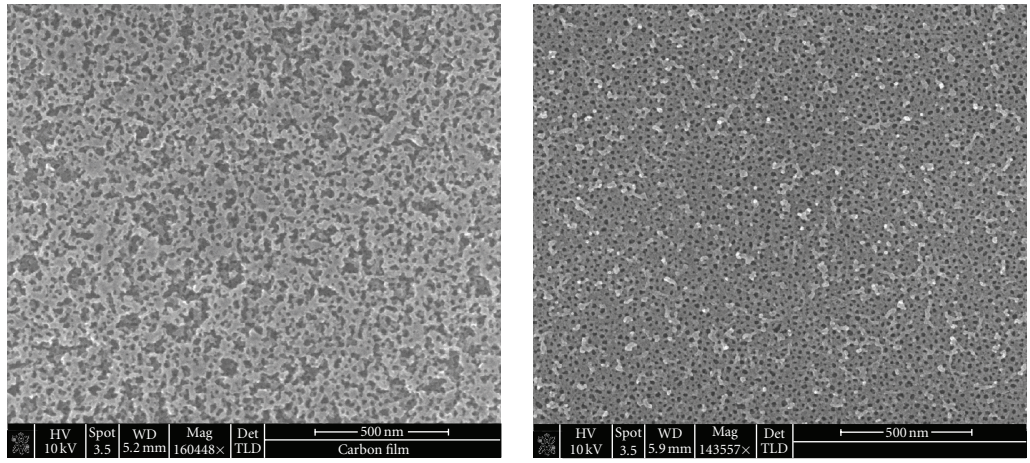

(a) (b)

Figure 8: SEM images of nanoporous TiO_2 layer fabricated by the anodization of FCVA-deposited Ti thin film on a quartz substrate.

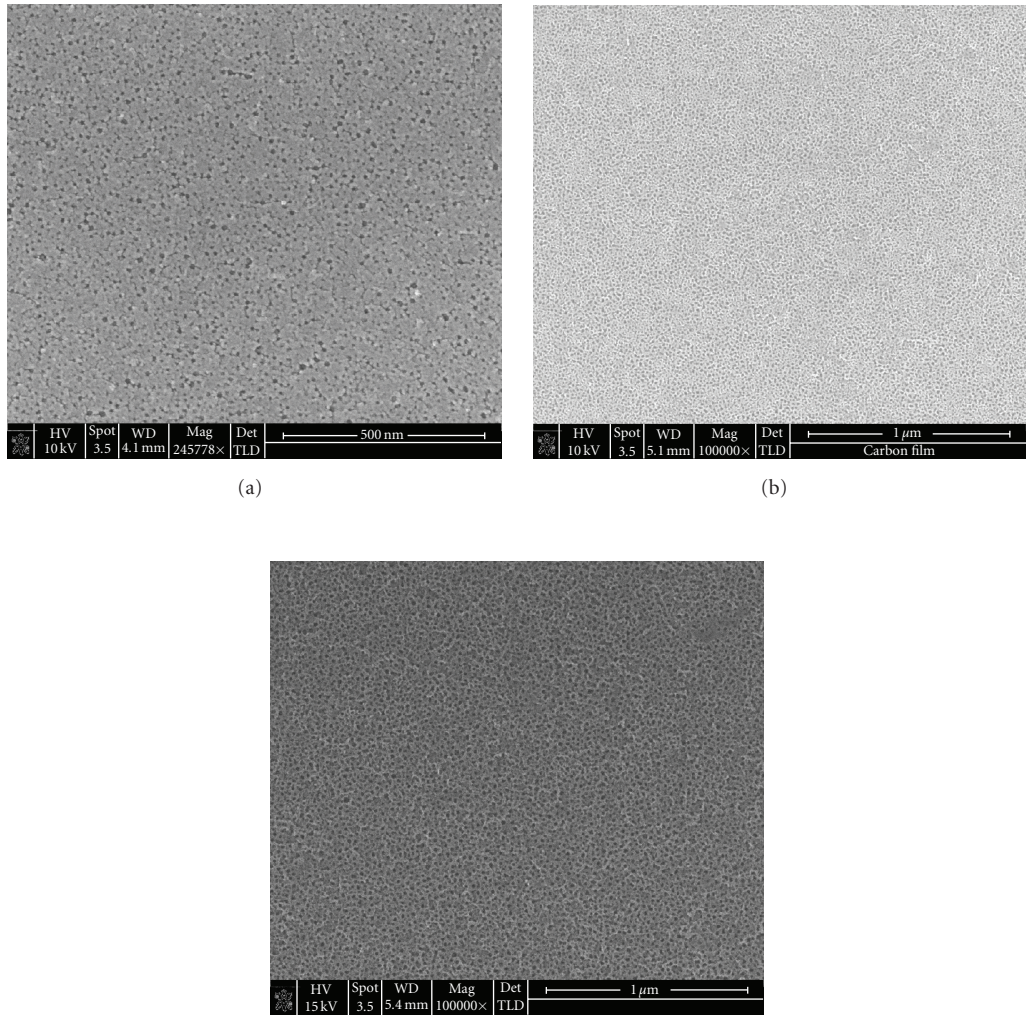

(a) (b)

(c)

Figure 9: SEM images of nanoporous TiO_2 layer fabricated by the anodization of FCVA-deposited Ti thin film at different potentials: (a) 2 V, (b) 10 V, and (c) 20 V.

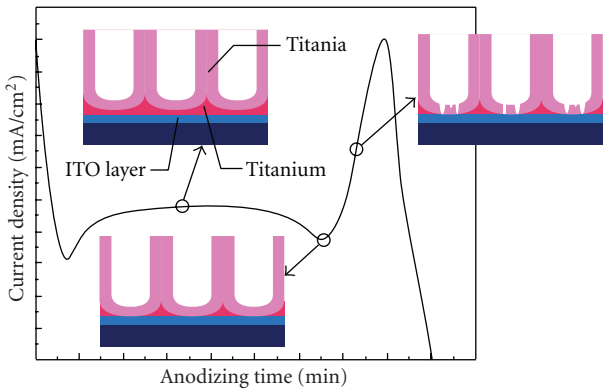

FIGURE 10: Schematic diagram of ITO-based Ti thin film during the anodization process.

atmosphere inside the nanotube prevents the fully filling of dye-contained solution into the nanotube which causes a very limited adsorption at only the open mouth part. The second is that the remaining oxide layer at the bottom of the nanotubes increases the resistance and decreases the FF of the device. The third problem is the repeated annealing process which results in an increase of FTO resistance.

Paulose et al. [71] reported another reflective type DSSCs based on titanium nanotube arrays anodized from Ti sheet. The anodization was performed in KF electrolyte at 25 V with a tube length of 6 μm and a diameter and a wall thickness of 110 nm and 20 nm, respectively. The nanotubes were annealed at 580°C for 6 hours for crystallization. In this type of solar cell, a 1.3 nm Pt coated TCO glass was used as the counter electrode, and the other structure is exactly the same as the device prepared by Mor et al. [69, 70]. The effective area of this device was 0.4 cm^2. When illuminated at AM-1.5 (100 mW/cm^2), J_{sc} of 15 mA/cm^2 and V_{oc} of 0.84 V were obtained. The FF for such device was 0.43 with a total photoconversion efficiency of 5.44%. Paulose pointed out that the low FF was ascribed to the thick barrier layer at the bottom of the nanotubes. They also supposed that the stepwise potential decrease, which is widely used in the anodization of Al to reduce the thickness of barrier layer, could also be used in this case to improve the properties of this device.

4.3. Gas Sensors. As a functional semiconductor material, TiO_2 is widely used in the field of gas sensors. Nanostructural TiO_2 attracts an increasing interest due to its large surface area since the sensing process is mainly a surface process between the gas molecules and metal oxide surface.

Many investigations showed that highly ordered nanotube arrays have excellent response to hydrogen gas at room temperature [72–76]. According to these reports, there is no significant relationship between the sensitivity and the length of the nanotubes since the sensitivity only increases from 7 to 8.7 when the nanotube length increases from 380 nm to 1 μm. However, due to the large surface area of the nanotubular structure, the sensitivity of nanotube-based sensors is much higher than that of compact TiO_2 thin film sensors. Further discussion on nanoporous TiO_2-based gas sensors will be presented later in this paper.

4.4. Electrochromic Devices. Ghicov et al. [77] reported the electrochromic properties of titanium nanotubes fabricated by anodization in a 1 M H_3PO_4 + 1 M NaOH + 0.5 wt% HF electrolyte at 20 V. The prepared nanotube has a length of 1 μm, a diameter of 100 nm, and a wall thickness of 10 nm. The H^+ intercalation changes the energy band structure of TiO_2 which causes the color change. Since the efficiency of ion intercalation and detercalation is closely related to the surface area, the large aspect ratio of titanium nanotubes provided a largely increased storage capability for H^+. They concluded that the anodic titanium nanotube will find its applications in the field of display devices, hydrogen storage as well as supercapacitors.

4.5. Biaoactive Materials. Yang et al. [78] and Oh et al. [79] reported the application of anodic titanium as a bioactive material. Their studies showed that phosphorite grows easily on the anodic titanium surface by immersing the samples into simulated body fluid (SBF), which means that anodization is one of the effective methods to prepare bioactive materials. Yang also reported that, with the incubation for 3 days, phosphorite only grows on samples anodized at high potentials (150 and/or 180 V) but not on that anodized at a low potential (90 V). They believed that the different surface morphologies obtained at different anodization potentials is the key factor for the phosphorite growth.

5. Fabrication of Nanoporous Anodic Titanium Thin Films

Since the applications of functional devices need some special requirements on the substrate, for example, optical devices need transparent substrates while surface acoustic wave (SAW) devices need piezoelectric substrates, more and more groups have focused their research interests on the fabrication of anodic films based on the anodization of titanium films on different substrates instead of titanium metal sheets/foils [49, 70, 72, 80–83]. Because the anodization is performed on titanium thin films, therefore, a variety of substrates can be chosen in the film deposition processes. As a result, the obtained anodic films with nanostructures can find wide potential applications in a variety of devices.

As we have discussed previously many technical problems need to be solved, and the growth mechanism of nanostructural anodic thin films needs to be investigated since thin films have different properties compared with the bulk materials. The limited thickness of thin films also needs to be considered during the anodization process. The investigation on the optimal thin film anodization parameters becomes highly important.

In this section, the study of nanoporous titanium thin films on different substrates including Si, ITO, and quartz will be presented based on the research outcome from the authors' research laboratory and their team. By investigating the *I-V* curves, anodizing potential, type of

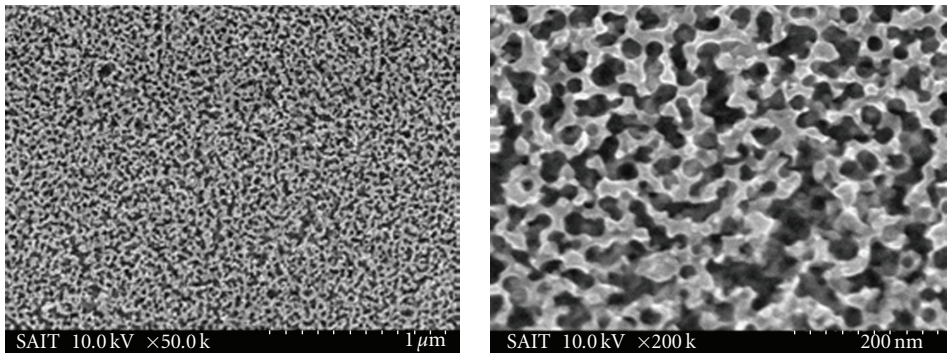

(a) (b)

Figure 11: SEM image of nanoporous Ti on ITO substrate.

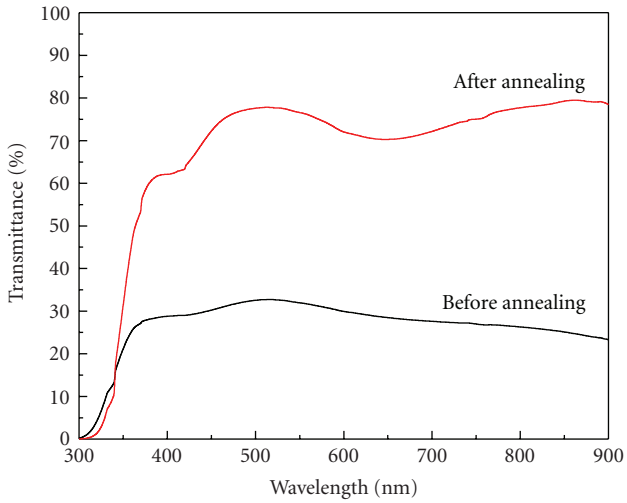

Figure 12: Transmittance spectra of ATO nanoporous thin films on ITO substrate before and after heat treatment.

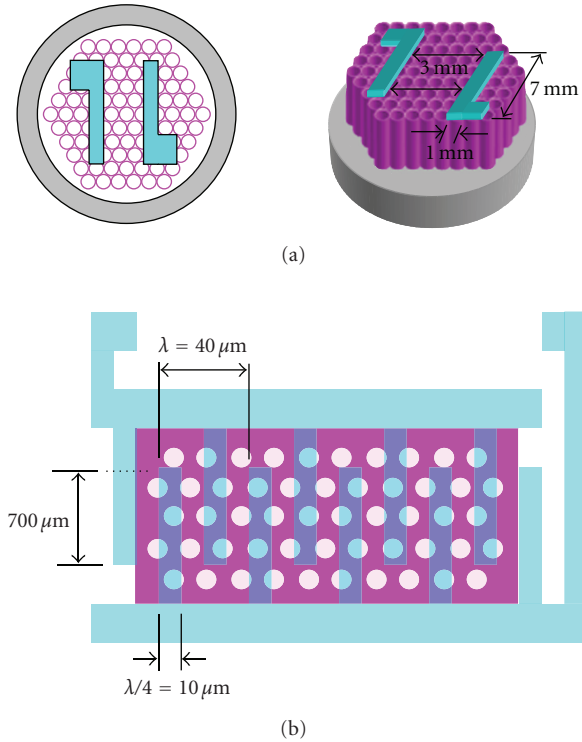

(a)

(b)

Figure 13: Schematic diagram of Anodic Titanium Oxide (ATO) nanotube-based gas sensors: (a) the first type and (b) the second type.

electrolyte, initial morphology of Ti films as well as their crystal structures, a growth mechanism is developed for the nanoporous/nanotube anodic thin films formation.

5.1. Experimental Procedure

5.1.1. Ti Thin Film Deposition

RF Sputtering. Ti films were deposited on a chosen substrate by RF magnetic sputtering. The base chamber pressure was below 9.0×10^{-6} Torr. During the deposition process, the argon gas pressure was 1.0×10^{-2} Torr. The distance between the target and sample was 50 mm, and the sputtering power was 100 W. No substrate heating was performed. The desired film thickness was in a range from 300 nm to 500 nm.

Filtered Cathodic Vacuum Arc (FCVA) Deposition. The source featured a water-cooled rotating M60-threaded copper base, which accepted a 70 mm diameter cathode (99.99% purity Ti for these experiments). The cathode was struck by a grounded mechanical striker to initiate the plasma. An arc current of 120 A (with an average arc power of 3 kW) was found to be sufficient to produce a stable plasma. For these experiments, a sample bias of −50 V was used. A magnetic filter was employed to prevent the deposition of macroparticles onto the sample, thereby minimizing surface roughness. The thickness of the film deposited in the process was approximately 300 nm.

5.1.2. Anodization. Before anodization, the specimen was degreased in acetone using an ultrasonic bath for several

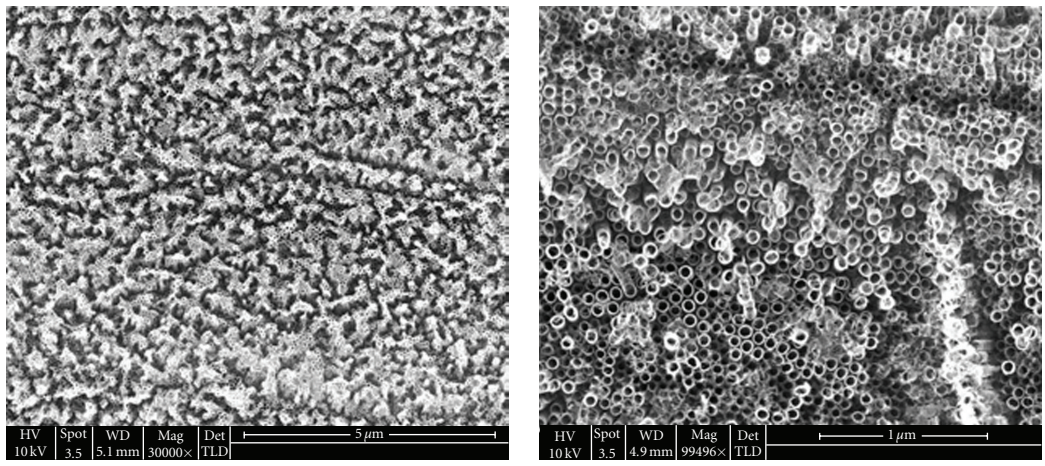

(a) (b)

Figure 14: SEM images of the ATO nanotube arrays for gas sensor.

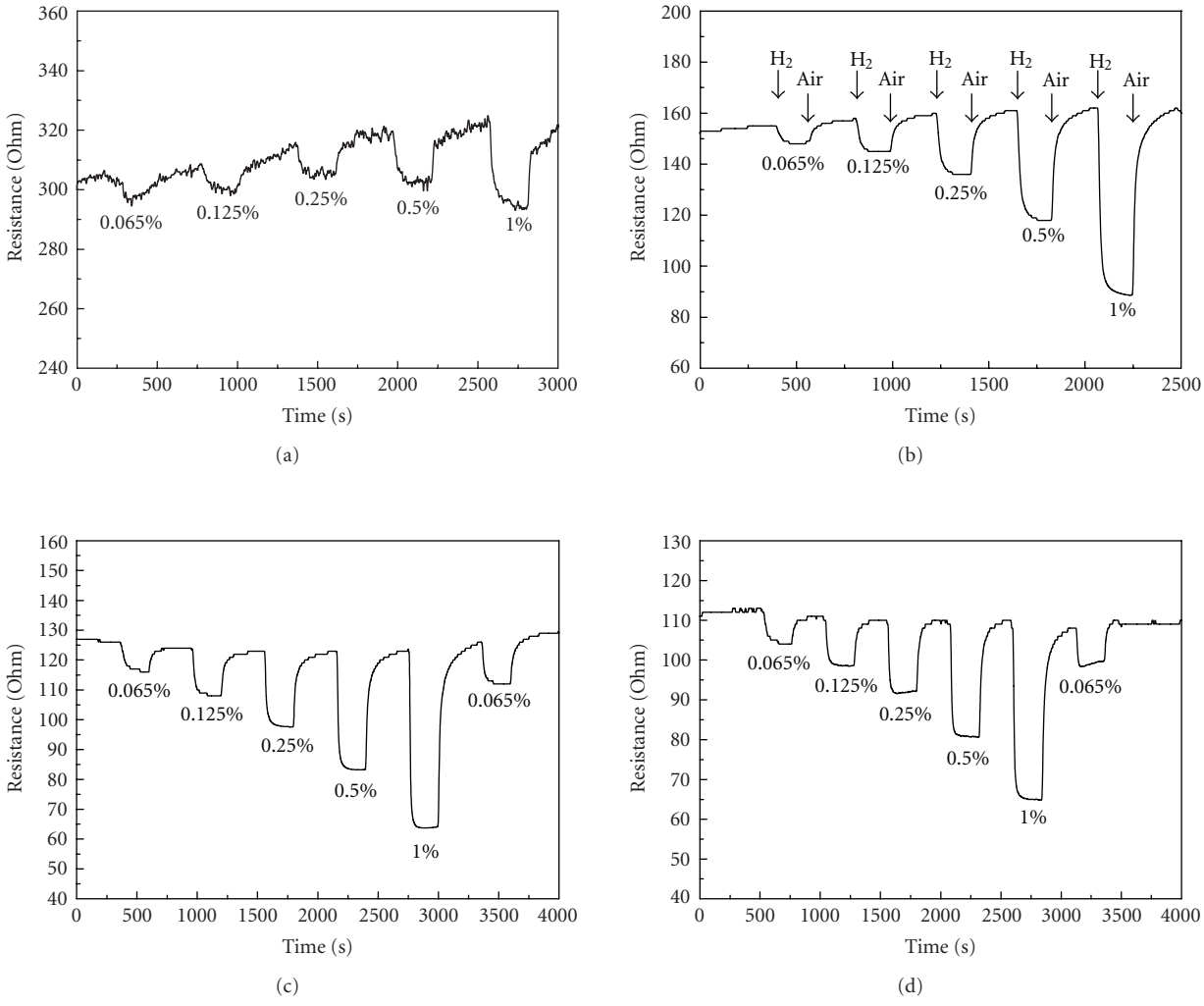

Figure 15: Dynamic response of ATO nanotube arrays-based gas sensor to H_2 at different working temperatures: (a) 90°C, (b) 160°C, (c) 190°C, and (d) 215°C.

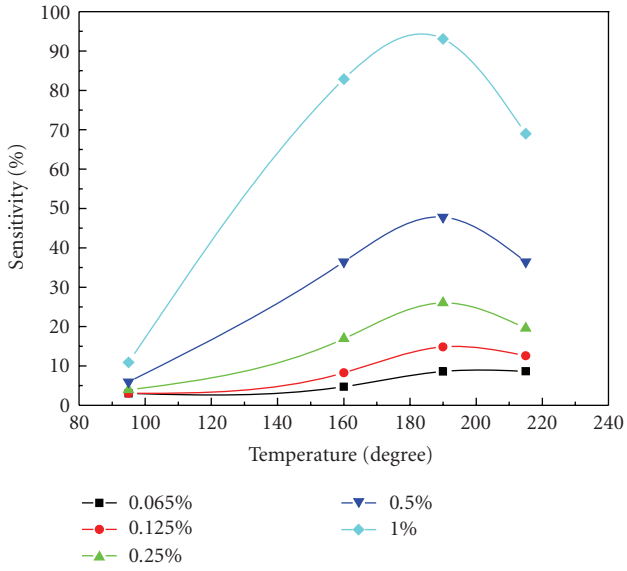

Figure 16: The relationship between sensitivity and working temperatures for the ATO nanotube arrays-based gas sensor.

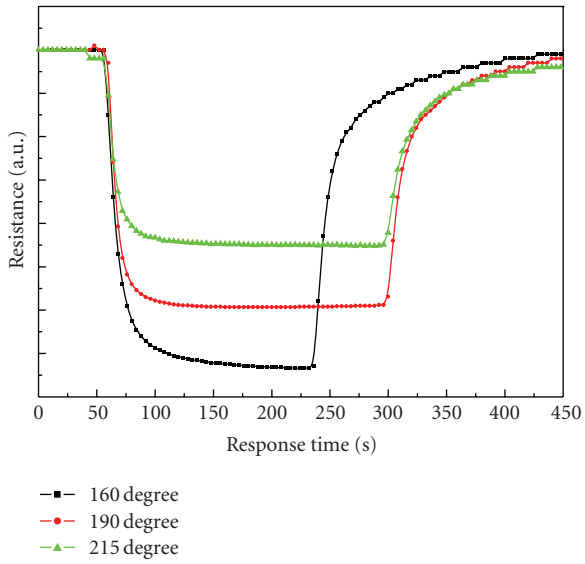

Figure 17: Response time for the ATO nanotube arrays-based gas sensor to H_2 (1%).

minutes and then rinsed in deionized water. No polishing process was adapted. The anodization was performed using a conventional two-electrode system. Silicon substrate with titanium film was attached to a silver rod that was used as the working electrode. A platinum sheet ($2 \times 1.5\,cm^2$) with a platinum wire was used as the counter-electrode. The distance between the working and counter-electrodes was kept at 3 cm. The anodization potential was applied using a potentiostat (Agilent E3645A) interfaced with a computer. The electrolyte was stirred using a magnetic flea during the anodization process.

5.1.3. Annealing. In order to investigate the crystallization, samples after anodization were annealed in a quartz tube furnace at different temperatures with the temperature ramp of 3°C/min. Either air or pure oxygen gas was used for annealing.

5.1.4. Characterization. The morphologies of microstructures were investigated using a field emission scanning electron microscope (SEM; JSM-6700F, JEOL Inc.). X-ray diffraction (XRD) analysis was performed using a Rigaku D/max 2550V diffractometer with Cu Kα radiation at 45 kV and 100 mA. UV-Vis spectrum was obtained by a UV-Vis spectrometer (SHIMADZU-23101PC).

5.2. Results and Discussion

5.2.1. Nanoporous Anodic Titanium Film and Its Growth Model. Figure 1 shows the typical SEM image of nanoporous anodic titanium thin film after anodization. Anodization was performed on Ti film (300 nm) sputtered on a Si substrate in a 0.5 wt% aqueous HF electrolyte at 3 V. The temperature was kept at 3°C using an ice bath during the process to prevent the oxide formed from being dissolved in acidic solution. The porous surface shows connecting pores with the average diameter of 25 nm and interpore distance of 40 nm.

Figure 2 shows the typical current density transient recorded during anodization under a constant voltage when self-organized pores were obtained. The pore formation process in anodic titanium oxide is similar to that of PAA, which can be divided into four stages.

(i) In the first stage, a compact oxide barrier layer is formed on the electrolyte–metal interface, which leads the current to decrease sharply due to the low conductivity of the metal oxide.

(ii) In the second stage, some cracks and narrow slits appear on the surface due to field-enhanced dissolution of the oxide layer. Diffusion of the electrolyte into such cracks enhances the dissolution rate compared with other areas, which enlarges the cracks and connects the neighboring cracks. Meanwhile, this process enlarges the interface between electrolyte and oxide layer which decreases the resistance and increases the anodizing current. In this stage, initial tiny pores are nuclear in the cracks, and therefore such cracks are named as "easy path".

(iii) The current reaches a stable state in the third stage, which corresponds to the random formation of porous structure in the slits and cracks. These slits and cracks extend over the whole surface area. Such a process is a competition between the pore formation and dissolution of the oxide layer. The stable state of the current density transient indicates that the pore formation reaches equilibrium with the pore dissolution.

(iv) In the fourth stage, when the dissolution rate is larger than the formation rate, the porous structure is consumed and current reduces.

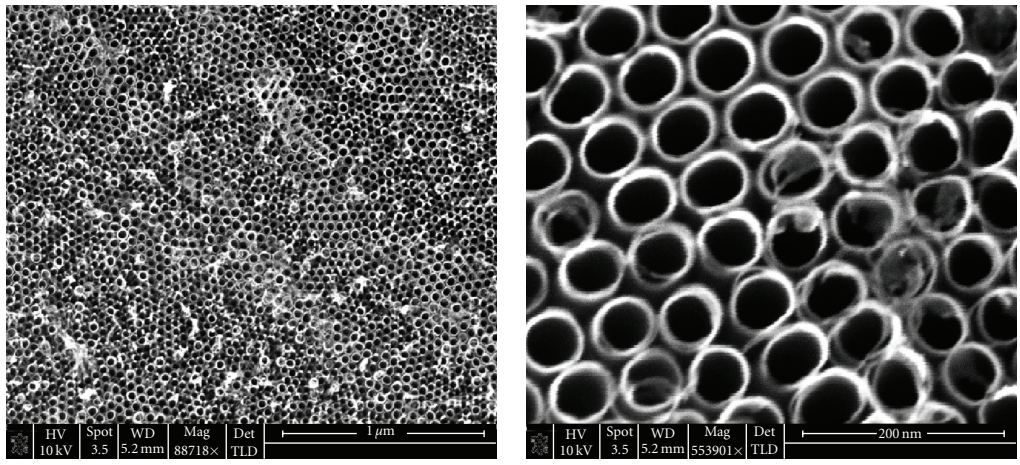

(a) (b)

Figure 18: SEM images of the highly ordered ATO nanotubes for the gas sensor.

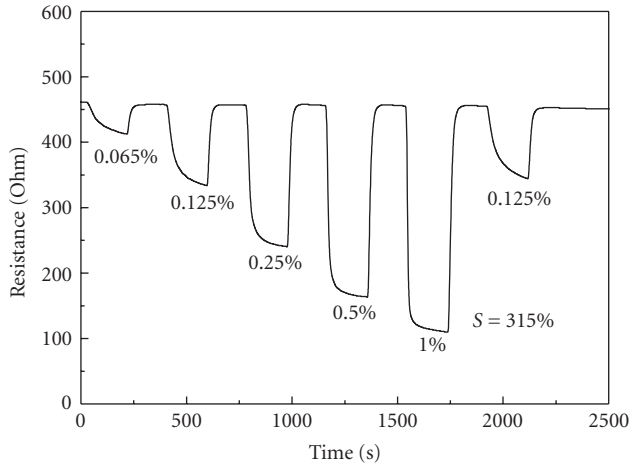

Figure 19: Dynamic response for the highly ordered ATO nanotube-based sensor to H_2.

5.2.2. Effect of Anodizing Conditions on the Morphologies

Anodizing Potential and Concentration of Electrolyte. We can assume that the formation of different surface structures is strongly correlated with the thickness of the compact oxide layer formed at the initial stage of the anodization process. There must be a threshold thickness above which the big corrosion pits form; when the thickness of the oxide layer is below the threshold, porous structure forms. According to the study of the anodic aluminum oxide nanoporous process, it is presumed that the compact titanium oxide layer formed at the initial of stage of the anodization process is in the range of 0.1–1 nm. The schematic diagrams of the formation processes for the two different structures are shown in Figures 3 and 4.

At a high anodizing potential, when the electric field is strong, a thick oxide layer forms due to large Ti ion dissolution and reprecipitation of hydroxide film. The oxide layer is compact with a considerable thickness (Figure 3(a)). Such a thick compact oxide layer (referred to as a "barrier layer") prevents the migration of OH^- under the electric field from the electrolyte to the metal/oxide interface. At the same time, it prevents the migration of Ti^{4+} ions from the metal/oxide interface to the electrolyte. This barrier layer protects the metal thin film from being etched away. When anodization continues, the fluoride ions will attack the defect sites on the surface of the barrier layer which cause small notches (Figure 3(b)). Electrolytes pour into the notches and accelerate their growth until the metal/oxide interface is reached (Figure 4(c)). The exposure of metal substrate to electrolyte causes the current transient to increase due to the sudden departure of Ti^{4+} ions from the metal substrate to the electrolyte. Soon, the bottom of the pits is covered by an oxide layer (repassivated), and hence the current transient decreases (Figure 3(d)). In addition, localized breakdowns may occur at the bottom of the pits, and new notches can be generated; this is followed by repassivation (Figures 3(e) and 3(f)). That may explain the formation of corrosion pits and why it always occurs with the current oscillations. Because of the barrier layer, the anodization can last for a long time and, the current oscillation is kept undamped.

When porous structures are formed at a low potential, the barrier layer formed at the beginning of anodization is much thinner than that for a high potential (Figure 4(a)). Microslits appear on the surface of the oxide layer; this is followed by the growth of pores, as the electric field intensity at the pore bottom is much higher than that at the walls due to their different curvatures. Titanium is etched at a higher rate near the bottom, which allows the formation of pores in the direction normal to the surface. At the same time, owing to the remaining thin oxide layer, the OH^- ions may migrate to the metal/oxide interface, followed by the formation of oxide. If the rates of oxide formation and dissolution at the bottom are equal, the thickness of the barrier layer is kept constant (Figures 4(b)–4(d)). The $j - t$ curve recorded in such a process (as shown in Figure 2) is quite smooth and

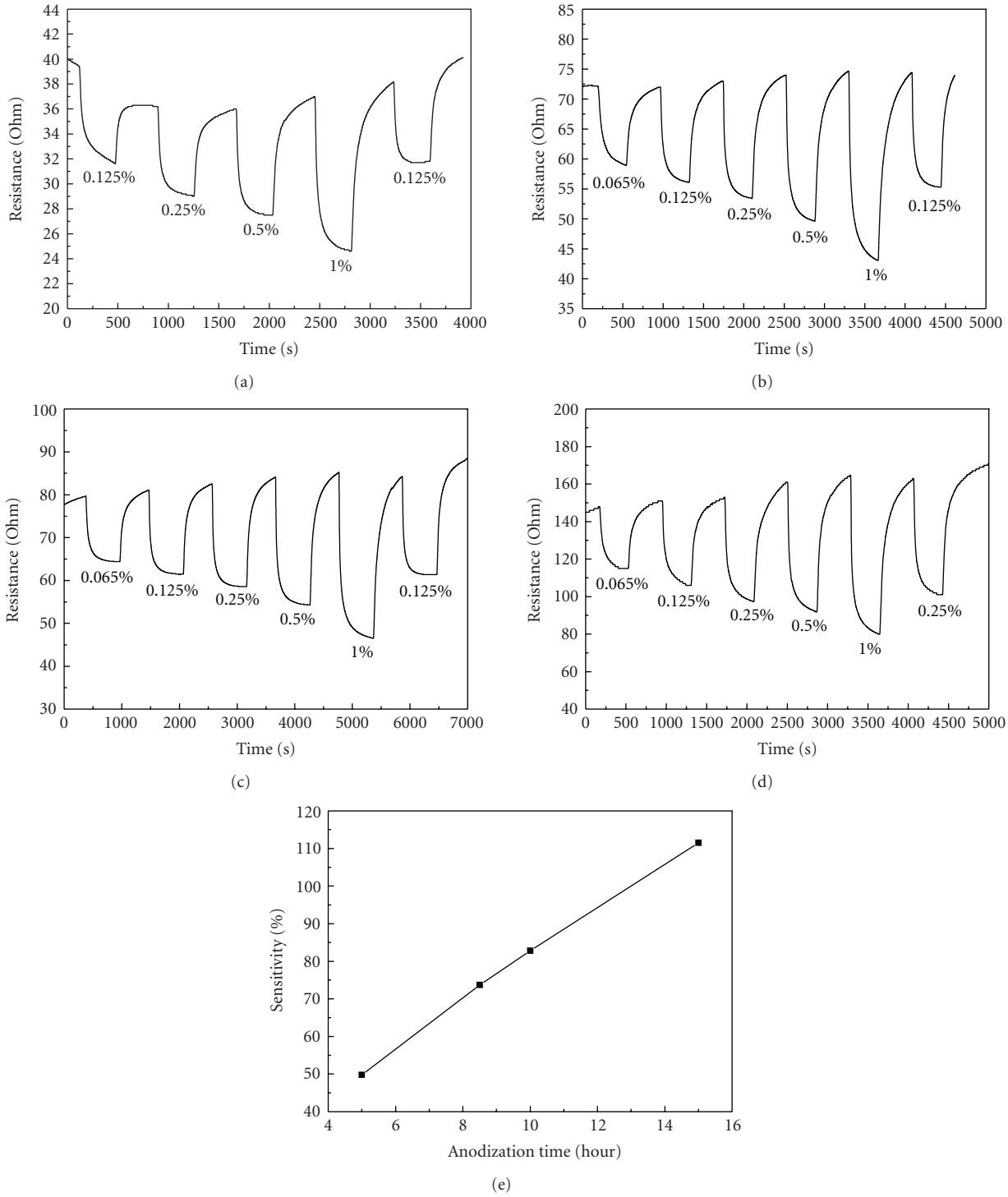

Figure 20: Dynamic response to H_2 of ATO nanotubes fabricated from different anodization time.

without oscillations which can be due to nondirect exposure of the metal substrate to the electrolyte.

The Film Smoothness. In the previous reports, acidic electrolytes were mainly utilized to obtain nanopores/nanotubes in the Ti thin films [72, 84–86] while the neutral electrolyte was widely used for the anodization of Ti foils [57–60]. This phenomenon is ascribed to be due to the differences of initial surface morphologies. A schematic diagram is presented in Figure 5, which explains the influence of the electric-field on the formation of the nanopores onto smooth and granular surfaces. When the potential is applied to a smooth surface, homogeneous distribution of the electric field was formed between the two electrodes (working and counter

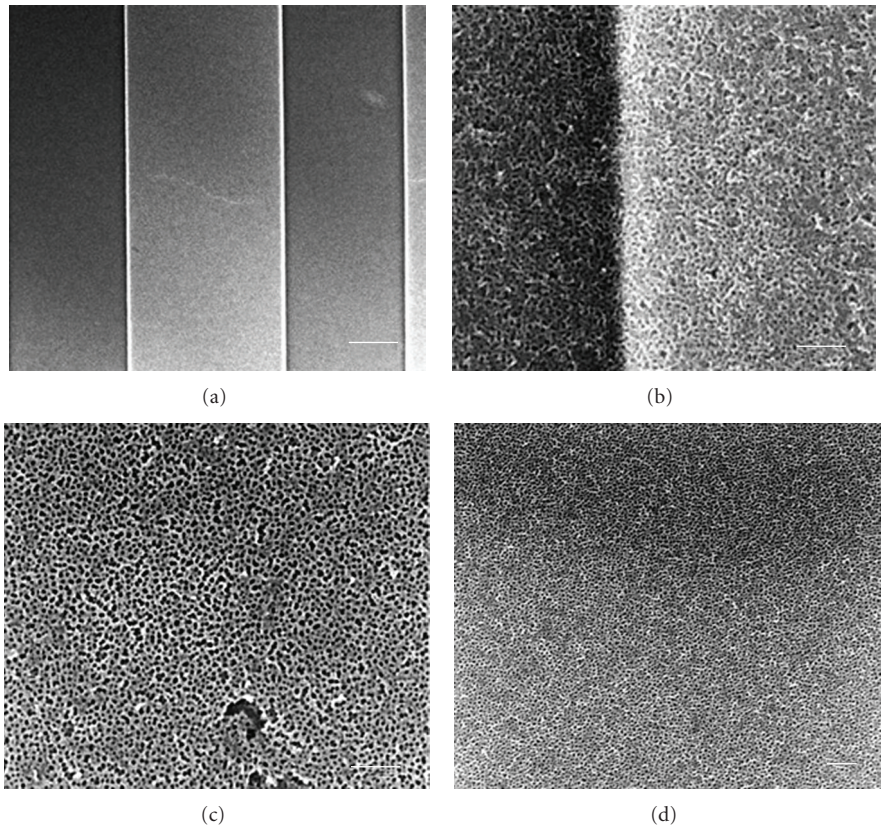

Figure 21: SEM image of nanoporous TiO_2 thin film on $LiNbO_3$ substrate. (a) SAW device, (b) the interface between Au electrode and $LiNbO_3$ substrate, (c) nanoporous thin film on $LiNbO_3$ substrate and, (d) nanoporous thin film on Au electrode.

electrode). Thereby, nanopores form homogeneously on the whole surface induced by the electric field. In the case of the granular surface, however, because of the large curvatures in the boundary of the connected grains, the electric field distribution is far from homogeneous which results in preferential nanopore growths in these parts, and randomly distributed nanopores are formed eventually.

Thereby the formation of uniform nanostructures always corresponds to the smoothness of the initial surface morphology. It is well known that in order to obtain highly ordered AAO nanoporous structures, a pretreatment by electropolishing process in an acidic electrolyte is required, which helps to reduce the time (named as "initial time") cost for pore ordering in later anodization process. For titanium anodization, however, no effective prepolishing method has ever been used, neither mechanical nor electrochemical.

Figure 6 shows SEM images of the surface morphologies of Ti film deposited by RF sputtering before and after anodization in a neutral electrolyte (0.5 wt% NH_4F in EG solution). As can be seen in Figure 6(a), the film consists of randomly distributed grains. During the anodization process, this level of roughness generates inhomogeneous electric field distributions on the surface. As what we have discussed, pores are often quickly formed on surface sites with small radius of curvature, where a high electricfield density occurs (i.e., between grains). As can be seen in Figure 6(b) the morphology of the anodized surface is highly inhomogeneous.

In order to achieve a highly smooth Ti films, we used the Filtered Cathodic Vacuum Arc (FCVA) deposition technique. The SEM inspection of the FCVA-deposited Ti films revealed extremely low defect density and roughness. AFM was also used to confirm the low surface roughness of these Ti films prior to anodization. The RMS of the film with a thickness of 300 nm was found to be less than 0.5 nm over a 500×500 nm^2 surface area.

The anodization was firstly performed on the Ti thin films prepared by FCVA on quartz substrates in a neutral aqueous electrolyte containing 0.5 wt% NH_4F and 1 M $(NH_4)_2SO_4$. This anodization process was initially performed at 3°C, as previous work showed that homogeneous nanopores were obtained at low temperatures [84, 86]. Figure 8(a) shows an SEM image of the sample after anodization at 3 V. The anodization was carried out in two steps. In the initial step a less ordered structure was formed. While with the continuation of the anodization process this layer dissolved, and a nanoporous structure was formed. However, the initial layer still covered most of the surface. Apparently, the neutral electrolyte and the low temperature caused a low dissolution rate in this process. In order to obtain a smooth surface a higher temperature anodization process was used. At roomtemperature (20°C) the anodization was performed

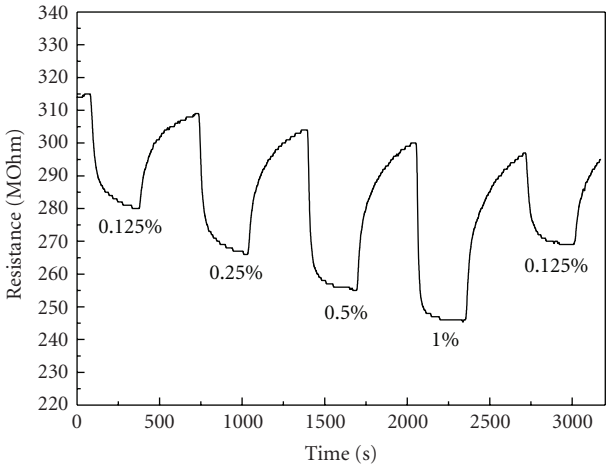

Figure 22: Dynamic response to H_2 of ATO nanoporous thin film-based gas sensors.

in the same electrolyte at 3 V, and the SEM image is shown in Figure 8(b). Ordered nanopores with a diameter in the range of 15–20 nm were clearly observed in the SEM image. Although anodized at room temperature, relatively thin Ti layers (<300 nm thickness) can be used as starting layers in this process as it produces regular pores without an extended activation etch.

Further anodization trials were conducted on Ti thin films deposited on quartz substrates by FCVA using 0.5 wt% NH_4F in ethylene glycol at room temperature (20°C). The SEM images of anodization performed at different potentials are shown in Figure 9. The sample shown in Figure 9(a) was anodized at 2 V for 1 hour resulting in the development of nanopores with diameters ranging from 5 nm to 8 nm. At 10 V, larger pores with diameters of approximately 12 nm–15 nm were obtained as shown in Figure 9(b). When anodization was performed at a potential of 20 V, the pores diameters were in the range from 15 nm to 20 nm (Figure 9(c)). It appears that at higher potentials the walls between pores are dissolved in many sites. These results reveal that the anodization on the FCVA-deposited Ti thin film can be performed in a potential range from 2 V to 15 V by using a neutral electrolyte at room temperature to obtain various pore diameters.

5.2.3. Transparent Conductive Substrates. Figure 10 shows a typical *I-V* curve recorded during the anodization process of titanium thin film on ITO glass. It can be seen that at the initial state, due to the formation of barrier layer and nucleation of nanopores, the anodic current experiences a decreasing process first, and then, followed by is increasing. When the pores grow steadily, anodic current keeps at a stable state. During this period, the nanopores reach the metal/ITO interface; because of the assumption of titanium metals, the anodic current grows to a minimum value again. However, after the exposure of ITO layer to the electrolyte, due to its dissolution, the current increases one more time until all the ITO is dissolved, and the current goes to zero. Thereby in order to guarantee the growth of nanopores without damaging the ITO layer, current monitoring is very important to stop the anodization when there is a second current increasing which indicates the dissolution of ITO layer.

Figure 11 shows the SEM images of ITO-based titanium thin film after anodization. The titanium film with a thickness of 300 nm was sputtered on ITO glass substrate. The anodization was performed in 0.5 wt% HF + 1 M H_2SO_4 electrolyte at 5 V in an ice water bath (~ 3°C). As discussed above, the anodization was ceased when the 2nd current increasing is seen. The anodic film presents a nanoporous structure with an average pore diameter of 20 nm. It is also observed that the neighboring pores are not connected with each other which are ascribed to the dissolution due to the low pH value and high anodization potential.

Annealing at 400°C in O_2 for 3 hours proves not only improving the crystallization of the anodic thin film (from amorphous to anatase) but also increasing its transparency from less than 30% to 75% as well, as shown in Figure 12. The change of transparency also reflects the change of crystallization, and its high transparency provides the potential applications in the optoelectronic devices.

6. Gas Sensing of Anodic Titanium Thin Films

6.1. Fabrication and Characterization of Gas Sensors. Two types of gas sensors were assembled. One was based on nanotubular titanium oxide anodized from titanium metal/foil,and the other was nanoporous titanium oxide thin film on $LiNbO_3$ substrate with Au electrodes.

The structure of the first type of sensor is shown in Figure 13(a), which uses nanotubular titanium oxide as the main part with effective area of 3.14 cm^2 (sphere shape with diameter of 1 cm). Two parallel Pt lines with a width and a length of 1 mm, 7 mm, respectively, were sputtered as the electrodes. The thickness of each electrode is 100 nm. The distance of the two electrodes is kept as 4 mm.

The second type of sensor is shown in Figure 13(b). It is based on a 64° YX $LiNbO_3$ substrate with 160 gold finger-pair electrodes. The periodicity and aperture width of the Au finger-pair are 40 μm and 700 μm, respectively. The titanium thin film was sputtered on the substrate followed by anodization.

For the dynamic response characterization of the first type of sensors, the resistance was measured by KEITHLEY 2001 multimeter, while for the second type of sensors, the frequency of surface acoustic wave (SAW) was recorded. In each testing cycle, the test chamber was filled by synthetic air first followed by filling of test gas with a given concentration through a multiflow controller and lasted for a desiring period. Finally, synthetic air was used to fill the chamber again.

6.2. Gas Sensing Properties of Anodic Nanotube TiO_2. Figure 14 shows the morphology of the titanium oxide nanotube arrays used as the first type of sensor. The anodization was performed in 0.5 wt% NH_4F-contained EG

electrolyte at 20 V for 12 hours followed by annealing in O_2 at 500°C for 6 hours. It is observed that a highly ordered nanotube arrays with average tube diameter of 50~70 nm were obtained after a "multistep" anodization process. The length of nanotubes is around 2~5 μm, that gives a high aspect ratio which is of significant importance in gas sensing applications.

Dynamic response of this type of sensor to H_2 with different concentrations is performed at 90, 160, 190, and 215°C (Figure 15). As an n-type semiconductor, when exposed in a reducing gas, the resistance of titanium oxide decreased. Therefore, the sensitivity of the sensor is defined as $S = (G_{gas} - G_{air})/G_{air}$, that is $S = (R_{air} - R_{gas})/R_{gas}$. G_{air}, G_{gas} represents the conductivity of titanium oxide nanotubes in the testing gas atmosphere. At lower temperature (90°C), unstable response is observed as shown in Figure 15(a). With the increasing of working temperature, more stable response is obtained with good repeatability (Figures 15(b), 15(c) and 15(d)). The relation between the sensitivity and working temperature is shown in Figure 16, from which we can observe that the sensitivity increases with the increasing of H_2 concentration regardless of the working temperature. However, such curve shows a sensitivity maximum with the increasing of working temperature and decreasing again. In our experiment, the optimal operating temperature of the sensor is at 190°C.

Figure 17 shows the quick response time for the titanium oxide nanotube-based sensor. It is observed that for either response time or recovery time, less than 10 seconds is required to reach 50% resistance change. Taken into consideration of the tube wall thickness (7~15 nm), the intercalation and detercalation of H_2 into the nanotubes are far much easier than in the thin films, which prolong the response and discovery times. Hence, the advantage of nanotubes for gas sensing is prominent.

Multistep anodization was performed to fabricate highly ordered TiO_2 nanotubes as shown in Figure 18. In this process, anodization was performed at a given condition followed by the removal of formed nanotubular structure in diluted HF solution and, then the sample was anodized again at the exactly same condition. The whole cycle was repeated one or two times until a much more ordered structure was obtained. H_2 sensor based on it was assembled and tested. The dynamic response is shown in Figure 19. We are pleased to find that when the sensor is working at 90°C, it presents extreme excellent stability compared with the previous normal nanotube-based sensor. Furthermore, the sensitivity (to 1.0% H_2) is as high as 315% while the sensitivity for the previous is only 11%. We ascribed such a high stability and sensitivity to the highly ordered nanostructure which enlarges the aspect ratio.

The change of sensitivity also occurs with the length of nanotubes, which can be manipulated by the anodizing time. Anodization was performed in same 0.5 wt% NH_4F electrolyte at 20 V for different anodization time, 5, 8.5, 10, and 15 hours, respectively. Dynamic responses to H_2 for nanotube-based sensors with different tube lengths are shown in Figures 20(a)–20(d), and the relation between sensitivity and anodizing time is shown in Figure 20(e). It can be seen that with the increasing of tube length, the base resistance increases, 37, 74, 82.4, and 156 Ω, respectively. The sensitivity also increases linearly with the anodizing time. Thereby it is ascribed to the increasing length of nanotubes which enlarges the aspect ratio (surface to volume area).

6.3. Nanoporous TiO_2 Thin Film-Based Gas Sensors. Figure 21 shows the morphologies of Ti thin film sputtered on $LiNbO_3$ substrate (with Au electrodes) after anodization. The anodization was performed in 0.5% $(NH_4)F$-contained EG electrolyte at 5 V. It can be observed that nanopores distribute homogeneously on the whole device surface, as shown in Figure 21(a). On the Au/ $LiNbO_3$ interface, because of the geometric step, the distribution of nanopores is less ordered, while on either $LiNbO_3$ substrate or Au electrode the distribution of nanopores is much better (Figures 21(c) and 21(d)). Before being used in gas sensors, the nanoporous thin film on substrate was annealed in O_2 at 400°C for 3 hours. The dynamic response of this type of sensor is shown in Figure 22, which presents a good sensitivity and stability.

7. Summaries

It was shown that due to their ordered and controllable structures, nanoporous/nanotubes semiconducting titanium oxide materials have great potential applications in various fields such as electronics, photoelectric conversion, photocatalysts and, low dimensional titanate-based perovskite ferroelectric materials and nanodevices.

In view of the above-mentioned aspects, we may come to the conclusion that the anodization technique is very effective and unique in fabricating nanostructural titanium. The anodization has been extended to the other metals such as W [87–91], Nb [92–95], Zr [96–99], Hf [100, 101], and Ni [102] and attracts more and more interests on fundamental studies and their various applications.

Generally speaking, as a newly developed method, there still remain lots of problems to be solved for the anodization of titanium. The growth mechanism of nanotubulr TiO_2, for instance, has been mostly derived from the anodization of aluminum oxide which cannot be completely acceptable. If the semiconducting property of titanium oxide is taken into consideration, in contrast to the insulating aluminum oxide, the chances are that the growth mechanism needs to be modified. Furthermore, just as the development of AAO, now that the morphology of anodic titanium has been further controlled, more efforts should be exerted to find practical applications. As a semiconductor material, titanium oxide has already attracted lots of interests. Due to the unique advantages provided by nanostructures, anodic titanium will further find its applications in more newly developed functional devices [84–86, 103–105]. In order to meet the increasing requirements for the potential applications, the anodization technique needs to be optimized. For instance, when anodization is performed on a titanium sheet, the metal substrate remained has the short-circuit problem which limits its applications in the electrical devices, while the opacity limits the applications in optical devices. As

a result, the fabrication of nanostructural thin films based on different substrates (Si, glass and organic flexible ones) becomes significantly important.

In this paper, we reviewed the fabrication of titanium oxide nanotube arrays, nanoporous thin films as well as their growth model and applications. Our research results showed that highly ordered titanium oxide nanotube arrays-based gas sensor has excellent response to H_2. By using "multistep anodization process", highly ordered nanotube arrays were obtained, and gas sensors based on such nanostructure presented a fast and stable response even at a low operating temperature of 90°C. Meanwhile, such sensors show very high sensitivity and present good dynamic response. In this paper, response to H_2 was presented as a case study.

Acknowledgment

This work was supported by the National Natural Science Foundation of China (NSFC, no. 50703047), China-Australia Special Scientific Research Fund, and Samsung Advanced Institute of Technology (SAIT), Republic of Korea.

References

[1] J. H. Wu, X. L. Wu, N. Tang, Y. F. Mei, and X. M. Bao, "Strong ultraviolet and violet photoluminescence from Si-based anodic porous alumina films," *Applied Physics A*, vol. 72, no. 6, pp. 735–737, 2001.

[2] T. Gao, G. Meng, Y. Tian, S. Sun, X. Liu, and L. Zhang, "Photoluminescence of ZnO nanoparticles loaded into porous anodic alumina hosts," *Journal of Physics: Condensed Matter*, vol. 14, no. 47, pp. 12651–12656, 2002.

[3] R. Kudrawiec, J. Misiewicz, L. Bryja, I. S. Molchan, and N. V. Gaponenko, "Photoluminescence investigation of porous anodic alumina with spin-on europium-containing titania sol-gel films," *Journal of Alloys and Compounds*, vol. 341, no. 1-2, pp. 211–213, 2002.

[4] R. Kudrawiec, A. Podhorodecki, N. Mirowska, et al., "Photoluminescence investigation of europium-doped alumina, titania and indium sol-gel-derived films in porous anodic alumina," *Materials Science and Engineering B*, vol. 105, no. 1–3, pp. 53–56, 2003.

[5] N. V. Gaponenko, I. S. Molchan, G. E. Thompson, et al., "Photoluminescence of Eu-doped titania xerogel spin-on deposited on porous anodic alumina," *Sensors and Actuators A*, vol. 99, no. 1-2, pp. 71–73, 2002.

[6] A. E. Gridnev and V. V. Chernyshev, "Periodic oscillations of luminescence intensity at the formation of anodic oxides on aluminum in oxalic acid," *Russian Journal of Electrochemistry*, vol. 40, no. 8, pp. 872–873, 2004.

[7] Y. Yamamoto, N. Baba, and S. Tajima, "Colored materials and photoluminescence centers in anodic film on aluminum," *Nature*, vol. 289, pp. 572–574, 1981.

[8] H. A. Lopez and P. M. Fauchet, "1.54 μm electroluminescence from erbium-doped porous silicon composites for photonic applications," *Physica Status Solidi A*, vol. 182, no. 1, pp. 413–418, 2000.

[9] Y. Zhao, D. Yang, C. Zhou, Q. Yang, and D. Que, "Photoluminescence properties of the composite of porous alumina and poly (2,5-dibutoxy-1,4 phenylenevinylene)," *Journal of Luminescence*, vol. 105, no. 1, pp. 57–60, 2003.

[10] R. Jia, Y. Shen, H. Luo, X. Chen, Z. Hu, and D. Xue, "Photoluminescence properties of morin and lysozyme molecules absorbed on anodic porous alumina membrane," *Applied Surface Science*, vol. 233, no. 1–4, pp. 343–351, 2004.

[11] Y. Du, W. L. Cai, C. M. Mo, J. Chen, L. D. Zhang, and X. G. Zhu, "Preparation and photoluminescence of alumina membranes with ordered pore arrays," *Applied Physics Letters*, vol. 74, no. 20, pp. 2951–2953, 1999.

[12] Z. Ling, S. Chen, J. Wang, and Y. Li, "Fabrication and properties of anodic alumina humidity sensor with through-hole structure," *Chinese Science Bulletin*, vol. 53, no. 2, pp. 183–187, 2008.

[13] N. D. Hoa, N. Van Quy, Y. Cho, and D. Kim, "An ammonia gas sensor based on non-catalytically synthesized carbon nanotubes on an anodic aluminum oxide template," *Sensors and Actuators B*, vol. 127, no. 2, pp. 447–454, 2007.

[14] D. Ding, Z. Chen, S. Rajaputra, and V. Singh, "Hydrogen sensors based on aligned carbon nanotubes in an anodic aluminum oxide template with palladium as a top electrode," *Sensors and Actuators B*, vol. 124, no. 1, pp. 12–17, 2007.

[15] G. Gorokh, A. Mozalev, D. Solovei, V. Khatko, E. Llobet, and X. Correig, "Anodic formation of low-aspect-ratio porous alumina films for metal-oxide sensor application," *Electrochimica Acta*, vol. 52, no. 4, pp. 1771–1780, 2006.

[16] T. Mukherjee, S. K. Hazra, and S. Basu, "Porous titania thin films grown by anodic oxidation for hydrogen sensors," *Materials and Manufacturing Processes*, vol. 21, no. 3, pp. 247–251, 2006.

[17] N. Negishi, T. Iyoda, K. Hashimoto, and A. Fujishima, "Preparation of transparent TiO_2 thin-film photocatalyst and its photocatalytic activity," *Chemistry Letters*, pp. 841–842, 1995.

[18] C. Lieber, "Nanowire-based photovoltaics build small powerful solar cells," *Advanced Materials & Processes*, vol. 166, p. 24, 2008.

[19] Y. Gao, M. Nagai, T.-C. Chang, and J.-J. Shyue, "Solution-derived ZnO nanowire array film as photoelectrode in dye-sensitized solar cells," *Crystal Growth and Design*, vol. 7, no. 12, pp. 2467–2471, 2007.

[20] E. Enache-Pommer, J. E. Boercker, and E. S. Aydil, "Electron transport and recombination in polycrystalline TiO_2 nanowire dye-sensitized solar cells," *Applied Physics Letters*, vol. 91, no. 12, Article ID 123116, 2007.

[21] C.-H. Ku and J.-J. Wu, "Electron transport properties in ZnO nanowire array/nanoparticle composite dye-sensitized solar cells," *Applied Physics Letters*, vol. 91, no. 9, Article ID 093117, 2007.

[22] J.-J. Wu, G.-R. Chen, H.-H. Yang, C.-H. Ku, and J.-Y. Lai, "Effects of dye adsorption on the electron transport properties in ZnO-nanowire dye-sensitized solar cells," *Applied Physics Letters*, vol. 90, no. 21, 2007.

[23] U. Bach, D. Lupo, P. Comte, et al., "Solid-state dye-sensitized mesoporous TiO_2 solar cells with high photon-to-electron conversion efficiencies," *Nature*, vol. 395, no. 6702, pp. 583–585, 1998.

[24] P. Zhou, D. Xue, H. Luo, and X. Chen, "Fabrication, structure, and magnetic properties of highly ordered prussian blue nanowire arrays," *Nano Letters*, vol. 2, no. 8, pp. 845–847, 2002.

[25] S. Yang, H. Zhu, D. Yu, Z. Jin, S. Tang, and Y. Du, "Preparation and magnetic property of Fe nanowire array," *Journal of Magnetism and Magnetic Materials*, vol. 222, no. 1-2, pp. 97–100, 2000.

[26] D. H. Qin, L. Cao, Q. Y. Sun, Y. Huang, and H. L. Li, "Fine magnetic properties obtained in FeCo alloy nanowire arrays," *Chemical Physics Letters*, vol. 358, no. 5-6, pp. 484–488, 2002.

[27] Y. W. Wang, L. D. Zhang, G. W. Meng, X. S. Peng, Y. X. Jin, and J. Zhang, "Fabrication of ordered ferromagnetic-nonmagnetic alloy nanowire arrays and their magnetic property dependence on annealing temperature," *Journal of Physical Chemistry B*, vol. 106, no. 10, pp. 2502–2507, 2002.

[28] X. Y. Zhang, G. H. Wen, Y. F. Chan, R. K. Zheng, X. X. Zhang, and N. Wang, "Fabrication and magnetic properties of ultrathin Fe nanowire arrays," *Applied Physics Letters*, vol. 83, no. 16, pp. 3341–3343, 2003.

[29] C. W. Wang, Y. Peng, S. L. Pan, H. L. Zhang, and H. L. Li, "Mossbauer spectrum studies of magnetic anisotropy of alpha-Fe nanowire arrays in alumina template," *Acta Physica Sinica*, vol. 48, pp. 2146–2150, 1999.

[30] X. Y. Yuan, G. S. Wu, T. Xie, Y. Lin, and L. D. Zhang, "Self-assembly synthesis and magnetic studies of Co-P alloy nanowire arrays," *Nanotechnology*, vol. 15, no. 1, pp. 59–61, 2004.

[31] H. Gao, C. Mu, F. Wang, et al., "Field emission of large-area and graphitized carbon nanotube array on anodic aluminum oxide template," *Journal of Applied Physics*, vol. 93, no. 9, pp. 5602–5605, 2003.

[32] S.-H. Jeong and K.-H. Lee, "Fabrication of the aligned and patterned carbon nanotube field emitters using the anodic aluminum oxide nano-template on a Si wafer," *Synthetic Metals*, vol. 139, no. 2, pp. 385–390, 2003.

[33] N. I. Tatarenko and A. M. Mozalev, "Geometry and element composition of a nanoscale field emission array formed by self-organization in porous anodic aluminum oxide," *Solid-State Electronics*, vol. 45, no. 6, pp. 1009–1016, 2001.

[34] W. J. Yu, Y. S. Cho, G. S. Choi, and D. Kim, "Patterned carbon nanotube field emitter using the regular array of an anodic aluminium oxide template," *Nanotechnology*, vol. 16, no. 5, pp. S291–S295, 2005.

[35] P.-L. Chen, J.-K. Chang, C.-T. Kuo, and F.-M. Pan, "Field emission of carbon nanotubes on anodic aluminum oxide template with controlled tube density," *Applied Physics Letters*, vol. 86, no. 12, Article ID 123111, pp. 1–3, 2005.

[36] D. W. Kang and J. S. Suh, "Fabrication temperature effect of the field emission from closed and open tip carbon nanotube arrays fabricated on anodic aluminum oxide films," *Journal of Applied Physics*, vol. 96, no. 9, pp. 5234–5238, 2004.

[37] S.-H. Jeong and K.-H. Lee, "Field emission properties of low-density carbon nanotubes prepared on anodic aluminum-oxide template," *Journal of the Korean Physical Society*, vol. 45, no. 2, pp. L252–L255, 2004.

[38] S. I. Cho, W. J. Kwon, S.-J. Choi, et al., "Nanotube-based ultrafast electrochromic display," *Advanced Materials*, vol. 17, no. 2, pp. 171–175, 2005.

[39] P. Hoyer, "Formation of a titanium dioxide nanotube array," *Langmuir*, vol. 12, no. 6, pp. 1411–1413, 1996.

[40] T. Kasuga, M. Hiramatsu, A. Hoson, T. Sekino, and K. Niihara, "Formation of titanium oxide nanotube," *Langmuir*, vol. 14, no. 12, pp. 3160–3163, 1998.

[41] M. Zhang, Y. Bando, and K. Wada, "Sol-gel template preparation of TiO_2 nanotubes and nanorods," *Journal of Materials Science Letters*, vol. 20, no. 2, pp. 167–170, 2001.

[42] V. Zwilling, M. Aucouturier, and E. Darque-Ceretti, "Anodic oxidation of titanium and TA6V alloy in chromic media. An electrochemical approach," *Electrochimica Acta*, vol. 45, no. 6, pp. 921–929, 1999.

[43] V. Zwilling, E. Darque-Ceretti, A. Boutry-Forveille, D. David, M. Y. Perrin, and M. Aucouturier, "Structure and physicochemistry of anodic oxide films on titanium and TA6V alloy," *Surface and Interface Analysis*, vol. 27, no. 7, pp. 629–637, 1999.

[44] D. Gong, C. A. Grimes, O. K. Varghese, et al., "Titanium oxide nanotube arrays prepared by anodic oxidation," *Journal of Materials Research*, vol. 16, no. 12, pp. 3331–3334, 2001.

[45] G. K. Mor, O. K. Varghese, M. Paulose, N. Mukherjee, and C. A. Grimes, "Fabrication of tapered, conical-shaped titania nanotubes," *Journal of Materials Research*, vol. 18, no. 11, pp. 2588–2593, 2003.

[46] C. Ruan, M. Paulose, O. K. Varghese, G. K. Mor, and C. A. Grimes, "Fabrication of highly ordered TiO_2 nanotube arrays using an organic electrolyte," *Journal of Physical Chemistry B*, vol. 109, no. 33, pp. 15754–15759, 2005.

[47] G. K. Mor, M. A. Carvalho, O. K. Varghese, M. V. Pishko, and C. A. Grimes, "A room-temperature TiO_2-nanotube hydrogen sensor able to self-clean photoactively from environmental contamination," *Journal of Materials Research*, vol. 19, no. 2, pp. 628–634, 2004.

[48] G. K. Mor, O. K. Varghese, M. Paulose, and C. A. Grimes, "A self-cleaning, room-temperature titania-nanotube hydrogen gas sensor," *Sensor Letters*, vol. 1, pp. 42–46, 2003.

[49] G. K. Mor, K. Shankar, M. Paulose, O. K. Varghese, and C. A. Grimes, "Enhanced photocleavage of water using titania nanotube arrays," *Nano Letters*, vol. 5, no. 1, pp. 191–195, 2005.

[50] R. Beranek, H. Hildebrand, and P. Schmuki, "Self-organized porous titanium oxide prepared in H_2SO_4/HF electrolytes," *Electrochemical and Solid-State Letters*, vol. 6, no. 3, pp. B12–B14, 2003.

[51] J. M. Macak, H. Tsuchiya, and P. Schmuki, "High-aspect-ratio TiO_2 nanotubes by anodization of titanium," *Angewandte Chemie International Edition*, vol. 44, no. 14, pp. 2100–2102, 2005.

[52] J. M. MacAk, K. Sirotna, and P. Schmuki, "Self-organized porous titanium oxide prepared in Na_2SO_4/NaF electrolytes," *Electrochimica Acta*, vol. 50, no. 18, pp. 3679–3684, 2005.

[53] S. Bauer, S. Kleber, and P. Schmuki, "TiO_2 nanotubes: tailoring the geometry in H_3PO_4/HF electrolytes," *Electrochemistry Communications*, vol. 8, no. 8, pp. 1321–1325, 2006.

[54] Q. Cai, M. Paulose, O. K. Varghese, and C. A. Grimes, "The effect of electrolyte composition on the fabrication of self-organized titanium oxide nanotube arrays by anodic oxidation," *Journal of Materials Research*, vol. 20, no. 1, pp. 230–236, 2005.

[55] G. K. Mor, O. K. Varghese, M. Paulose, K. Shankar, and C. A. Grimes, "A review on highly ordered, vertically oriented TiO_2 nanotube arrays: fabrication, material properties, and solar energy applications," *Solar Energy Materials and Solar Cells*, vol. 90, no. 14, pp. 2011–2075, 2006.

[56] J. M. Macak and P. Schmuki, "Anodic growth of self-organized anodic TiO_2 nanotubes in viscous electrolytes," *Electrochimica Acta*, vol. 52, no. 3, pp. 1258–1264, 2006.

[57] J. M. Macak, H. Tsuchiya, L. Taveira, S. Aldabergerova, and P. Schmuki, "Smooth anodic TiO_2 nanotubes," *Angewandte Chemie International Edition*, vol. 44, no. 45, pp. 7463–7465, 2005.

[58] L. V. Taveira, J. M. Macak, H. Tsuchiya, L. F. P. Dick, and P. Schmuki, "Initiation and growth of self-organized TiO_2 nanotubes anodically formed in $NH_4F/(NH_4)_2SO_4$ electrolytes," *Journal of the Electrochemical Society*, vol. 152, no. 10, pp. B405–B410, 2005.

[59] C. Richter, Z. Wu, E. Panaitescu, R. J. Willey, and L. Menon, "Ultrahigh-aspect-ratio titania nanotubes," *Advanced Materials*, vol. 19, no. 7, pp. 946–948, 2007.

[60] H. Tsuchiya, J. M. Macak, L. Taveira, et al., "Self-organized TiO_2 nanotubes prepared in ammonium fluoride containing acetic acid electrolytes," *Electrochemistry Communications*, vol. 7, no. 6, pp. 576–580, 2005.

[61] C. Ruan, M. Paulose, O. K. Varghese, and C. A. Grimes, "Enhanced photoelectrochemical-response in highly ordered TiO_2 nanotube-arrays anodized in boric acid containing electrolyte," *Solar Energy Materials and Solar Cells*, vol. 90, no. 9, pp. 1283–1295, 2006.

[62] O. K. Varghese, D. Gong, M. Paulose, C. A. Grimes, and E. C. Dickey, "Crystallization and high-temperature structural stability of titanium oxide nanotube arrays," *Journal of Materials Research*, vol. 18, no. 1, pp. 156–165, 2003.

[63] K.-N. P. Kumar, K. Keizer, A. J. Burggraaf, T. Okubo, and H. Nagamoto, "Textural evolution and phase transformation in titania membranes: II supported membranes," *Journal of Materials Chemistry*, vol. 3, no. 11, pp. 1151–1159, 1993.

[64] O. K. Varghese, M. Paulose, K. Shankar, G. K. Mor, and C. A. Grimes, "Water-photolysis properties of micron-length highly-ordered titania nanotube-arrays," *Journal of Nanoscience and Nanotechnology*, vol. 5, no. 7, pp. 1158–1165, 2005.

[65] O. K. Varghese and C. A. Grimes, "Appropriate strategies for determining the photoconversion efficiency of water photoelectrolysis cells: a review with examples using titania nanotube array photoanodes," *Solar Energy Materials and Solar Cells*, vol. 92, no. 4, pp. 374–384, 2008.

[66] G. K. Mor, H. E. Prakasam, O. K. Varghese, K. Shankar, and C. A. Grimes, "Vertically oriented Ti-Fe-O nanotube array films: toward a useful material architecture for solar spectrum water photoelectrolysis," *Nano Letters*, vol. 7, no. 8, pp. 2356–2364, 2007.

[67] K. Shankar, G. K. Mor, H. E. Prakasam, et al., "Highly-ordered TiO_2 nanotube arrays up to 220 μm in length: use in water photoelectrolysis and dye-sensitized solar cells," *Nanotechnology*, vol. 18, no. 6, Article ID 065707, 11 pages, 2007.

[68] M. Paulose, G. K. Mor, O. K. Varghese, K. Shankar, and C. A. Grimes, "Visible light photoelectrochemical and water-photoelectrolysis properties of titania nanotube arrays," *Journal of Photochemistry and Photobiology A*, vol. 178, no. 1, pp. 8–15, 2006.

[69] G. K. Mor, K. Shankar, M. Paulose, O. K. Varghese, and C. A. Grimes, "Use of highly-ordered TiO_2 nanotube arrays in dye-sensitized solar cells," *Nano Letters*, vol. 6, no. 2, pp. 215–218, 2006.

[70] G. K. Mor, O. K. Varghese, M. Paulose, and C. A. Grimes, "Transparent highly ordered TiO_2 nanotube arrays via anodization of titanium thin films," *Advanced Functional Materials*, vol. 15, no. 8, pp. 1291–1296, 2005.

[71] M. Paulose, K. Shankar, O. K. Varghese, G. K. Mor, B. Hardin, and C. A. Grimes, "Backside illuminated dye-sensitized solar cells based on titania nanotube array electrodes," *Nanotechnology*, vol. 17, no. 5, pp. 1446–1448, 2006.

[72] G. K. Mor, O. K. Varghese, M. Paulose, K. G. Ong, and C. A. Grimes, "Fabrication of hydrogen sensors with transparent titanium oxide nanotube-array thin films as sensing elements," *Thin Solid Films*, vol. 496, no. 1, pp. 42–48, 2006.

[73] M. Paulose, O. K. Varghese, G. K. Mor, C. A. Grimes, and K. G. Ong, "Unprecedented ultra-high hydrogen gas sensitivity in undoped titania nanotubes," *Nanotechnology*, vol. 17, no. 2, pp. 398–402, 2006.

[74] O. K. Varghese, D. Gong, M. Paulose, K. G. Ong, E. C. Dickey, and C. A. Grimes, "Extreme changes in the electrical resistance of titania nanotubes with hydrogen exposure," *Advanced Materials*, vol. 15, no. 7-8, pp. 624–627, 2003.

[75] O. K. Varghese, D. Gong, M. Paulose, K. G. Ong, and C. A. Grimes, "Hydrogen sensing using titania nanotubes," *Sensors and Actuators B*, vol. 93, no. 1–3, pp. 338–344, 2003.

[76] Y. Shimizu, N. Kuwano, T. Hyodo, and M. Egashira, "High H_2 sensing performance of anodically oxidized TiO_2 film contacted with Pd," *Sensors and Actuators B*, vol. 83, no. 1–3, pp. 195–201, 2002.

[77] A. Ghicov, H. Tsuchiya, R. Hahn, J. M. MacAk, A. G. Munoz, and P. Schmuki, "TiO_2 nanotubes: H^+insertion and strong electrochromic effects," *Electrochemistry Communications*, vol. 8, no. 4, pp. 528–532, 2006.

[78] B. Yang, M. Uchida, H.-M. Kim, X. Zhang, and T. Kokubo, "Preparation of bioactive titanium metal via anodic oxidation treatment," *Biomaterials*, vol. 25, no. 6, pp. 1003–1010, 2004.

[79] H.-J. Oh, J.-H. Lee, Y. Jeong, Y.-J. Kim, and C.-S. Chi, "Microstructural characterization of biomedical titanium oxide film fabricated by electrochemical method," *Surface and Coatings Technology*, vol. 198, no. 1–3, pp. 247–252, 2005.

[80] S.-Z. Chu, S. Inoue, K. Wada, S. Hishita, and K. Kumshima, "Self-organized nanoporous anodic titania films and ordered titania nanodots/nanorods on glass," *Advanced Functional Materials*, vol. 15, no. 8, pp. 1343–1349, 2005.

[81] X. Yu, Y. Li, W. Ge, Q. Yang, N. Zhu, and K. Kalantar-Zadeh, "Formation of nanoporous titanium oxide films on silicon substrates using an anodization process," *Nanotechnology*, vol. 17, no. 3, pp. 808–814, 2006.

[82] Y. D. Premchand, T. Djenizian, F. Vacandio, and P. Knauth, "Fabrication of self-organized TiO_2 nanotubes from columnar titanium thin films sputtered on semiconductor surfaces," *Electrochemistry Communications*, vol. 8, no. 12, pp. 1840–1844, 2006.

[83] J. M. Macak, H. Tsuchiya, S. Berger, S. Bauer, S. Fujimoto, and P. Schmuki, "On wafer TiO_2 nanotube-layer formation by anodization of Ti-films on Si," *Chemical Physics Letters*, vol. 428, no. 4–6, pp. 421–425, 2006.

[84] K. S. Raja, M. Misra, and K. Paramguru, "Formation of self-ordered nano-tubular structure of anodic oxide layer on titanium," *Electrochimica Acta*, vol. 51, no. 1, pp. 154–165, 2005.

[85] R. P. Vitiello, J. M. Macak, A. Ghicov, H. Tsuchiya, L. F. P. Dick, and P. Schmuki, "N-doping of anodic TiO_2 nanotubes using heat treatment in ammonia," *Electrochemistry Communications*, vol. 8, no. 4, pp. 544–548, 2006.

[86] A. Ghicov, J. M. Macak, H. Tsuchiya, et al., "Ion implantation and annealing for an efficient N-doping of TiO_2 nanotubes," *Nano Letters*, vol. 6, no. 5, pp. 1080–1082, 2006.

[87] N. Mukherjee, M. Paulose, O. K. Varghese, G. K. Mor, and C. A. Grimes, "Fabrication of nanoporous tungsten oxide by galvanostatic anodization," *Journal of Materials Research*, vol. 18, no. 10, pp. 2296–2299, 2003.

[88] H. Tsuchiya, J. M. Macak, I. Sieber, et al., "Self-organized porous WO_3 formed in NaF electrolytes," *Electrochemistry Communications*, vol. 7, no. 3, pp. 295–298, 2005.

[89] S. Berger, H. Tsuchiya, A. Ghicov, and P. Schmuki, "High photocurrent conversion efficiency in self-organized porous

WO_3," *Applied Physics Letters*, vol. 88, no. 20, Article ID 203119, 2006.

[90] J. Choi, Y.-B. Park, and A. Scherer, "Fabrication of a tungsten master stamp using self-ordered porous alumina," *Nanotechnology*, vol. 16, no. 9, pp. 1655–1659, 2005.

[91] N. R. de Tacconi, C. R. Chenthamarakshan, G. Yogeeswaran, et al., "Nanoporous TiO_2 and WO_3 films by anodization of titanium and tungsten substrates: influence of process variables on morphology and photoelectrochemical response," *Journal of Physical Chemistry B*, vol. 110, no. 50, pp. 25347–25355, 2006.

[92] I. Sieber, H. Hildebrand, A. Friedrich, and P. Schmuki, "Formation of self-organized niobium porous oxide on niobium," *Electrochemistry Communications*, vol. 7, no. 1, pp. 97–100, 2005.

[93] J. Choi, J. H. Lim, S. C. Lee, J. H. Chang, K. J. Kim, and M. A. Cho, "Porous niobium oxide films prepared by anodization in HF/H_3PO_4," *Electrochimica Acta*, vol. 51, no. 25, pp. 5502–5507, 2006.

[94] J. Choi, J. H. Lim, J. Lee, and K. J. Kim, "Porous niobium oxide films prepared by anodization-annealing-anodization," *Nanotechnology*, vol. 18, no. 5, Article ID 055603, 6 pages, 2007.

[95] K. Kovacs, G. Kiss, M. Stenzel, and H. Zillgen, "Anodic oxidation of niobium sheets and porous bodies heat-treatment of the Nb/Nb-oxide system," *Journal of the Electrochemical Society*, vol. 150, no. 8, pp. B361–B366, 2003.

[96] H. Tsuchiya, J. M. Macak, I. Sieber, and P. Schmuki, "Self-organized high-aspect-ratio nanoporous zirconium oxides prepared by electrochemical anodization," *Small*, vol. 1, no. 7, pp. 722–725, 2005.

[97] H. Tsuchiya and P. Schmuki, "Thick self-organized porous zirconium oxide formed in H_2SO_4/NH_4F electrolytes," *Electrochemistry Communications*, vol. 6, no. 11, pp. 1131–1134, 2004.

[98] K. Yasuda and P. Schmuki, "Electrochemical formation of self-organized zirconium titanate nanotube multilayers," *Electrochemistry Communications*, vol. 9, no. 4, pp. 615–619, 2007.

[99] K. Yasuda and P. Schmuki, "Control of morphology and composition of self-organized zirconium titanate nanotubes formed in $(NH_4)_2SO_4/NH_4F$ electrolytes," *Electrochimica Acta*, vol. 52, no. 12, pp. 4053–4061, 2007.

[100] H. Tsuchiya and P. Schmuki, "Self-organized high aspect ratio porous hafnium oxide prepared by electrochemical anodization," *Electrochemistry Communications*, vol. 7, no. 1, pp. 49–52, 2005.

[101] T. Shobha, C. S. N. Sarma, K. S. Sastry, and C. H. Anjaneyulu, "Anodization of hafnium in phosphate baths: radio tracer studies," *Bulletin of Electrochemistry*, vol. 17, no. 11, pp. 519–522, 2001.

[102] S.-Z. Chu, K. Wada, S. Inoue, S.-I. Todoroki, Y. K. Takahashi, and K. Hono, "Fabrication and characteristics of ordered Ni nanostructures on glass by anodization and direct current electrodeposition," *Chemistry of Materials*, vol. 14, no. 11, pp. 4595–4602, 2002.

[103] J. M. Macak, H. Tsuchiya, A. Ghicov, and P. Schmuki, "Dye-sensitized anodic TiO_2 nanotubes," *Electrochemistry Communications*, vol. 7, no. 11, pp. 1133–1137, 2005.

[104] W.-J. Lee, M. Alhoshan, and W. H. Smyrl, "Titanium dioxide nanotube arrays fabricated by anodizing processes," *Journal of the Electrochemical Society*, vol. 153, no. 11, pp. B499–B505, 2006.

[105] K. Zhu, N. R. Neale, A. Miedaner, and A. J. Frank, "Enhanced charge-collection efficiencies and light scattering in dye-sensitized solar cells using oriented TiO_2 nanotubes arrays," *Nano Letters*, vol. 7, no. 1, pp. 69–74, 2007.